



**HAL**  
open science

# Robust control of a wind conversion system based on a hybrid excitation synchronous generator: A comparison between $H_\infty$ and CRONE controllers

Amina Mseddi, Sandrine Le Ballois, Helmi Aloui, Lionel Vido

## ► To cite this version:

Amina Mseddi, Sandrine Le Ballois, Helmi Aloui, Lionel Vido. Robust control of a wind conversion system based on a hybrid excitation synchronous generator: A comparison between  $H_\infty$  and CRONE controllers. *Mathematics and Computers in Simulation*, 2019, 158, pp.453-476. 10.1016/j.matcom.2018.11.004 . hal-02977670

**HAL Id: hal-02977670**

**<https://hal.science/hal-02977670>**

Submitted on 21 Oct 2021

**HAL** is a multi-disciplinary open access archive for the deposit and dissemination of scientific research documents, whether they are published or not. The documents may come from teaching and research institutions in France or abroad, or from public or private research centers.

L'archive ouverte pluridisciplinaire **HAL**, est destinée au dépôt et à la diffusion de documents scientifiques de niveau recherche, publiés ou non, émanant des établissements d'enseignement et de recherche français ou étrangers, des laboratoires publics ou privés.



Distributed under a Creative Commons Attribution - NonCommercial 4.0 International License

# Robust control of a Wind Conversion System based on a Hybrid Excitation Synchronous Generator: a comparison between $H_\infty$ and CRONE controllers

Amina Mseddi<sup>1,2</sup>, Sandrine Le Ballois<sup>1</sup>, Helmi Aloui<sup>2</sup>, Lionel Vido<sup>1</sup>

1. SATIE Laboratory, University of Cergy-Pontoise, 5 Mail Gay Lussac, 95031 Cergy-Pontoise, France

2. Laboratory of advanced Electronic Systems & Sustainable Energy, ISEM team, ENET'COM, Sfax, Tunisia

Tel : +33/644072717

E-mail: amina.mseddi90@gmail.com (corresponding author)

**Abstract** - This paper deals with a Wind Conversion System (WCS) based on a Hybrid Excitation Synchronous Generator (HESG) connected to an isolated load. The set is modeled under Matlab-Simulink. To ensure an efficient and reliable use of the system, a tight control remains vital. In fact, the dynamic equations of a turbine are strongly nonlinear as are the ones of a HESG; most of the system parameters are highly uncertain, and, at last, a WCS is always affected by disturbance sources such as load variances, harmonics, mechanical vibrations... To address these problems, robust control methods must be adopted. In this paper, two strategies for the control of variable speed wind turbine are investigated. First, an  $H_\infty$  controller is implemented. Then, a second-generation CRONE controller is designed. The performance of the two regulators is compared with respect to the tracking of the optimal rotation speed, the attenuation of the mechanical vibration and the robustness to the uncertainty of the parameters, using time-domain simulations. It has been found that the CRONE controller is more robust to parameters uncertainty and minimizes the fluctuations of the torsional torque and the generator's angular velocity. Finally, an experimental validation of the velocity controllers is presented to complete the simulation results and fully validate the chosen approach.

**Keywords** – WCS, HESG,  $H_\infty$  controller, 2<sup>nd</sup> generation CRONE controller, Optimal power tracking, Robustness

## 1. Introduction

Faced with fossil fuels depletion, their high cost and some pollution concerns, on the one hand, and with the worldwide demand for the reduction of carbon dioxide emissions and for the nature conservation, on the other hand, the use of renewable energies such as solar, geothermal and wind is now necessary. Among these alternatives, wind power is one of the most cost-effective. It is also one of the cleanest: while producing energy, wind turbines do not pollute neither the waters, nor the soils, and they don't propagate any greenhouse gas effects [1] [2].

However, because of the stochastic nature of the wind and the inevitable uncertainties of a WCS, wind turbines have operated with a low efficiency for many years. Previously, classical controllers such as P, PI, and PID based on linearized models were used [3] [4] [5]. Nowadays, the design of robust controllers with a capability of tracking smoothly and more efficiently the optimal wind extracted energy is of great interest for the wind power industry.

Among the different methods investigated in recent years, gain-scheduled controllers have been widely used for the control of variable speed wind turbines [6] [7], while using quasi-LPV models [8]. Adaptive algorithms [9], model predictive control [10], fuzzy logic approach [11] and predictive control using linear matrix inequalities [12] have also been applied to maximize the wind's extracted power. Yet, in most of these works, the implemented control strategy was validated and tested in a specific operating region, either the second area where the turbine is operated with an optimal efficiency or the third area where the wind extracted power must be limited (Fig 1). Likewise, several researchers have compared the performance of linear and nonlinear control methods [5] [13]. The effectiveness of the  $H_\infty$  regulator in the field of wind conversion systems' control has also been proved in many works [1] [14]. A comparison between LQG control and  $H_\infty$  control established in [15] proved that both controllers have the same performance regarding power generation and another comparative study, established in [1], has validated the performance of the  $H_\infty$  control method compared to a classical PID regulator.

In this work, the optimal power tracking in area 2 (Fig 1), as well as the limitation of the generator speed in area 3, of the considered structure, is ensured by an internal current loop and an external speed loop. A PI controller is designed for the current loop. Then, robust control techniques are applied in order to regulate the generator velocity loop. An  $H_\infty$  controller based on the Normalized Coprime Factors robust stabilization problem is implemented and tested in both partial and full load regimes. Furthermore, a second-generation CRONE controller is tested and compared to the  $H_\infty$  controller.

The CRONE controller, known as a robust controller is widely used in small passenger vehicles such as in [16] [17]. To the author’s knowledge, this work is the first is to propose a description and a validation of the CRONE control methodology for the whole operating range of a WCS. Indeed, few works dealt with the CRONE methodology in wind conversion system. Besides, the focus was mainly on the maximum power point tracking zone as in [18] and [19]. In these works, a very simple electrical model of a DC-excited synchronous generator was presented, whereas this work considers an advanced model of a HESG.

The comparison of the two robust controllers is made with respect to the maximization of the wind energy captured in the second operating zone and the minimization of the drive train transient loads in the third one. The robustness to parameters’ uncertainties and nonlinearities of the WCS for various wind profiles (including step ones and stochastic ones) is also evaluated for both controllers.

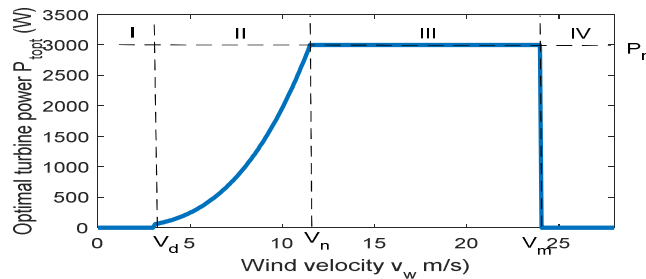


Fig 1: Shaft output power versus wind speed of a 3kW WCS

This research is also motivated by the use of a HESG in a wind conversion system as described in Fig 2. If many papers have dealt with the conception and the structural features of this innovative generator [16] [17], a few if any have evaluated its efficiency for a wind conversion system. Here, the focus is mainly on the development of an efficient and reliable overall control strategy for the hybrid generator in the wind energy field. In fact, in this type of generator, the excitation flux is created by permanent magnets and DC coils. This specificity adds a degree of freedom to the WCS architecture since the excitation winding current can be used as a control parameter. Here, the optimal rotation speed tracking is achieved by adjusting the excitation winding current. Moreover, a DC/DC converter, with very low power compared to the one necessary in a more conventional architecture, is sufficient for this control. This is the main asset of the proposed architecture.

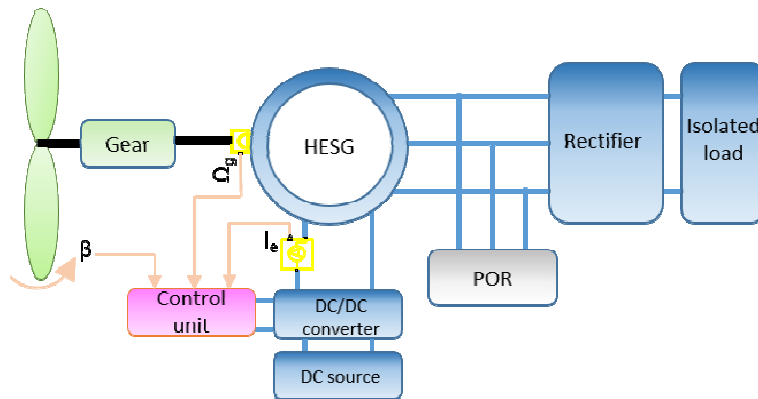


Fig 2: Architecture of the wind generator [18]

The paper is organized as follows. In section 2, a two masses mechanical model is presented to model the mechanical power transmission and an advanced electrical model taking into account generator harmonics and commutation effects



$$J_t \frac{d\Omega_t}{dt} = C_t - D_{ls} \left( \Omega_t - \frac{\Omega_g}{m_p} \right) - K_{ls} \left( \theta_t - \frac{\theta_g}{m_p} \right) - K_t \Omega_t \quad (5)$$

$$J_g \frac{d\Omega_g}{dt} = C_{em} - \frac{D_{ls}}{m_p} \left( \Omega_t - \frac{\Omega_g}{m_p} \right) - \frac{K_{ls}}{m_p} \left( \theta_t - \frac{\theta_g}{m_p} \right) - K_g \Omega_g \quad (6)$$

$\theta_g$  and  $\theta_t$  are the angular positions of the generator and of the turbine,  $J_g$  and  $J_t$  are the inertias of the generator and of the turbine,  $K_g$  and  $K_{ls}$  are respectively the generator and the slow shaft viscous friction coefficients and  $D_{ls}$  is the torsion coefficient of the slow shaft.

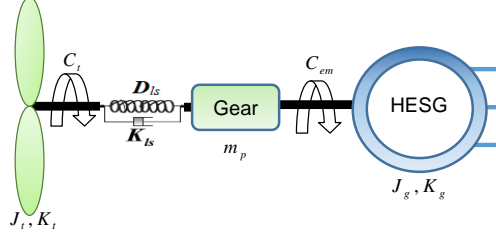


Fig 4: Two masses wind turbine model

Referring to (5) and (6), the generator speed can be expressed as in (7).

$$\Omega_g = \frac{f_2 s^2 + f_1 s + f_0}{e_3 s^3 + e_2 s^2 + e_1 s + e_0} \cdot \left[ \frac{(a_1 s + a_0) C_t}{b_2 s^2 + b_1 s + b_0} - C_{em} \right] \quad (7)$$

$$e_3 = J_g J_t m_p^2, e_2 = J_g (D_{ls} + K_t) m_p^2 + J_t (D_{ls} + K_g m_p^2), e_1 = K_{ls} J_t + J_g K_{ls} m_p^2 - D_{ls}^2 + (D_{ls} + K_g m_p^2) (D_{ls} + K_t)$$

Where:  $e_0 = (D_{ls} + K_t) K_{ls} - 2K_{ls} D_{ls} + (D_{ls} + K_g m_p^2) \cdot K_{ls}$ ,  $f_2 = J_t m_p^2$ ,  $f_1 = (D_{ls} + K_t) m_p^2$ ,  $f_0 = K_{ls} m_p^2$ ,  $a_1 = D_{ls} / m_p$ ,

$$a_0 = K_{ls} / m_p, b_2 = J_t, b_1 = D_{ls} + K_t, b_0 = K_{ls}$$

Fig 5 shows a couple of very flexible modes. The resonant frequency is noted  $w_r$  while the anti-resonant one is  $w_{a-r}$ . For some particular operating points, if the frequencies close to  $w_r$  and  $w_{a-r}$  are excited, the drive train may be threatened.

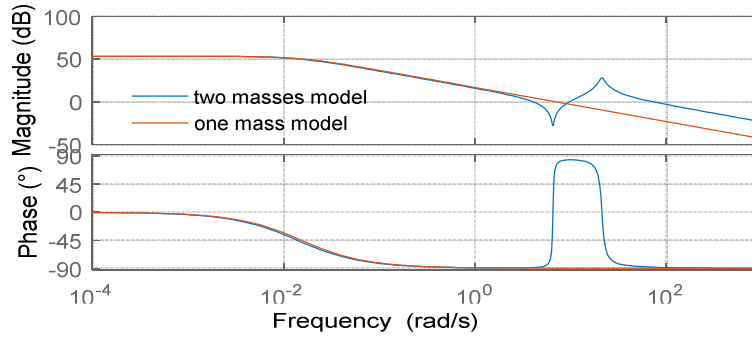


Fig 5: Bode diagram of  $\Delta\Omega_g / \Delta C_{em}$  of a 3kW WCS

While designing the velocity regulators, the drive train dynamics should be considered in order to guarantee the stability of the system and to avoid possible mechanical vibrations.

All the mechanical parameters of a 3kW WCS have been calculated using the scale down model method [24] [25]. In this approach, a mechanical parameter is calculated assuming a geometric similarity. Under the assumption of having the same blade tip speed ratio, two wind turbines are considered. The first one is the reference device. Its size is noted  $l'$ . The second one is the considered wind system and its size is noted  $l$ . The scale ratio noted "s" is calculated as in (8) where

$R'_p$  and  $R_p$  are known.

$$s = \frac{l'}{l} = \frac{R'_p}{R_p} \quad (8)$$

The slow shaft inertia, the turbine viscous friction coefficient, the slow shaft viscous friction coefficient and the torsion coefficient of the slow shaft are calculated as in (9) using three reference's turbines [26], [27] and [28]. Finally, a mean value is estimated. The corresponding values are provided in Table 1.

$$K_{ls} = \frac{K'_{ls}}{s^4} \quad D_{ls} = \frac{D'_{ls}}{s^4} \quad K_t = \frac{K'_t}{s^4} \quad J_t = \frac{J'_t}{s^5} \quad (9)$$

## 2.2. WCS electrical parts' models

The described parts include the HESG, the rectifier, the resistive load and the DC/DC converter.

### 2.2.1 HESG model

Among the inevitable uncertainties affecting in a significant way the power quality extracted from the wind, one can mention the generator's current harmonics [29]. It's a common practice to neglect this phenomenon. For instance, in [3], [14], [30] and [31], the generators are modeled in a d-q reference frame and a first harmonic model is considered. However, the distortion in the currents and armature voltages waveforms are due mainly to the harmonics which may cause torque rippling [21] and can lead to a bad reference tracking. Therefore, their impact on the wind extracted power needs further consideration.

To take into account the harmonics' effects, the HESG is modeled using the results presented in [32]. For example, for the "a" phase, the stator inductance is expressed as in (10), the mutual inductance as in (11) and the flux as in (12). A 18<sup>th</sup> order of Fourier series development is considered to express the stator inductances.

$$L = L_{s_0} + \sum_{h=1}^9 L_{s_{2h}} \cos(2hp\theta - \zeta_h) \quad (10)$$

$$M = M_{s_0} + \sum_{h=1}^9 M_{s_{2h}} \cos(2hp\theta - \zeta_h) \quad (11)$$

$$\phi_e = \sum_{h=0}^8 \phi_{a_{(2h+1)}} \cos(p\theta(2h+1) - \zeta_h) \quad (12)$$

$$\text{With } L_{s_0} = (L_d + L_q)/3, M_{s_0} = -L_{s_0}/3$$

$L_d$  and  $L_q$  are the d and q-axis inductances.  $\phi_a$  is the flux created by the magnets in the armature coils,  $\phi_e$  is the flux created by the magnets in the DC field excitation coils and  $p$  is the number of pole pairs.

Then, the generator is modeled in Concordia reference frame as in (13)-(17).

- Fluxes :

$$[\phi_2] = [L_2][I_2] + [M_{e2}]I_e + [\phi_{e2}] \quad (13)$$

$$\phi_e = [M_{e2}]^T [I_2] + L_e I_e + \phi_{ae} \quad (14)$$

- Voltages

$$[V_2] = R_s [I_2] + d[\phi_2]/dt \quad (15)$$

$$V_e = R_e I_e + d\phi_e/dt \quad (16)$$

- Electromagnetic torque

$$[C_{em}] = \frac{1}{2} [I_2]^T \frac{d[L_2]}{d\theta} [I_2] + [I_2]^T \frac{d[M_{e2}]}{d\theta} I_e + [I_2]^T \frac{d[\phi_{e2}]}{d\theta} \quad (17)$$

$$\text{Where: } \begin{aligned} [\phi_2]^T &= [\phi_{\alpha} \phi_{\beta}] & [V_2]^T &= [V_{\alpha} V_{\beta}] & [L_2] &= \begin{bmatrix} L_{\alpha} & M_{\alpha\beta} \\ M_{\alpha\beta} & L_{\beta} \end{bmatrix} & [M_{e2}]^T &= [M_{e\alpha} M_{e\beta}] \\ [\phi_{e2}]^T &= [\phi_{e\alpha} \phi_{e\beta}] & [I_2]^T &= [I_{\alpha} I_{\beta}] \end{aligned}$$

Here,  $L_{\alpha}$ ,  $L_{\beta}$ ,  $M_{\alpha\beta}$ ,  $M_{e\alpha}$ ,  $M_{e\beta}$  and  $M_{\alpha\beta}$  are analytically calculated then stocked in “lookup tables” so that the corresponding appropriate values may be generated according to the corresponding rotor’s position.

The electrical parameters of the generator were measured using the volt amperometric method (Fig 6). The corresponding values are given in Table 1.



Fig 6:  $L_d$ ,  $L_q$  and  $M$  measurement [32]

### 2.2.2 Converters and load models

A DC/DC converter controls the excitation coils of the HESG and the resistive load is connected to the WCS through a full bridge rectifier. SimPowerSystem tools are used for the modeling of the converters. They allow to take into account the commutations effects and test the controllers in a realistic environment [21].

The resistive load  $R_c$  is also implemented using SimPowerSystem blocks. A value of  $15\Omega$  is selected [33].

The nominal WCS’s parameters values and their variation ranges are summarized in Table 1.

Table 1: Parameters of the WCS

Parameter	Nominal value (variation range)	Parameter	Nominal value (variation range)
$\rho$ (Kg/m <sup>3</sup> )	1.2	$P_n$ (kW)	3
$K_t$ (kg.m <sup>2</sup> s <sup>-1</sup> )	0.055 ( $\pm 75\%$ )	$P$	6
$J_t$ (Kg.m <sup>2</sup> )	3.6	$M_e$ (mH)	1.1 (80-100%)
$R_p$ (m)	1.5	$L_d$ (mH)	5 (50-100%)
$m_p$	5	$L_q$ (mH)	9.2 (50-100%)
$D_{fs}$	0.8 ( $\pm 25\%$ )	$L_e$ (mH)	46 (50-100%)
$K_{fs}$	160(+48%/-34%)	$R_e$ ( $\Omega$ )	3 (100-150%)
$J_s$ (Kg.m <sup>2</sup> )	0.015	$R_s$ ( $\Omega$ )	0.87 (100-150%)
$\phi_a$ (mWb)	66 (80-100%)	$E_{DC}$ (V)	50
$G_0$	10	$V_{PM}$ (V)	5
$V_d$ (m/s)	3	$R_c$ ( $\Omega$ )	15
$V_n$ (m/s)	11.5	$V_m$ (m/s)	24

### 3. Control of the WCS

The control of a wind turbine must secure an appropriate reference tracking while minimizing its dynamic error. For a maximum power extraction using a HESG, the optimal turbine rotation speed may be adjusted by controlling the excitation current of the generator [14]. This section deals with the design of two robust controllers able to handle parametric uncertainties, external disturbance such as the wind’s brutal variations and that give a good closed-loop performance in all cases.

### 3.1. Open loop analysis

A typical output power versus wind speed for a WCS is illustrated in Fig 1. Based on this shape, and while knowing the turbine characteristics, a preliminary steady-state study allows to find the optimal turbine rotation speed and the optimal turbine torque to follow. They are illustrated in Fig 7 and Fig 8.

In fact, in order to operate with an optimal aerodynamic efficiency, a Maximum Power Point Tracker (MPPT) control algorithm has to be implemented. Below the rated wind speed  $V_n$ , the WCS rotation speed is adjusted to its optimal value as in (18). Since the turbine optimal characteristics ( $C_{pmax}$  and  $\lambda_{opt}$ ) are known, it is possible to apply the optimum tip speed ratio (TSR) method [34] to derive the optimal turbine velocity reference (18). Once the wind velocity surpasses  $V_n$ , the turbine rotation speed is limited to 450rpm in order to not surpass the WCS electrical and mechanical physical limits.

$$\Omega_{ref} = \lambda_{opt} \cdot V_w / R_p \quad (18)$$

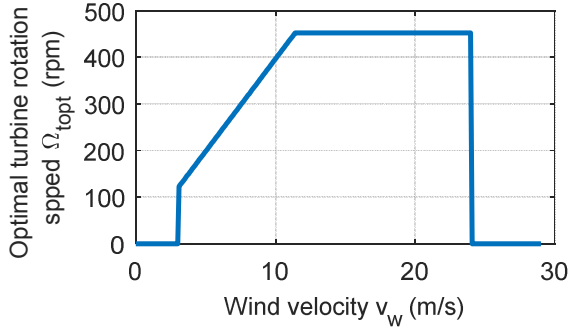


Fig 7: Optimal turbine torque versus wind speed

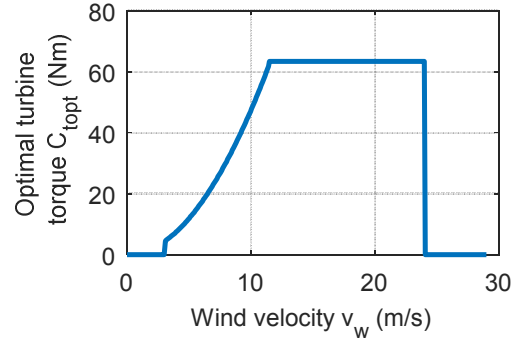


Fig 8: Optimal turbine speed versus wind speed

The open-loop analysis aims to find the variation range of the variables to control (the excitation current  $i_e$  and the rotation speed  $\Omega_g$ ) as a function of the system inputs (the turbine torque  $C_t$  and the control voltage  $v_{ec}$ ) and verify that each optimal point can be reached without violating the physical limits. The two inputs must vary between two maximal limits where:

$$V_{ecm} \leq 1 \quad \text{and} \quad 0 \leq C_t \leq C_m \quad (19)$$

Finally, the open loop study shows that each optimal point can be reached (Fig 9 and Fig 10).

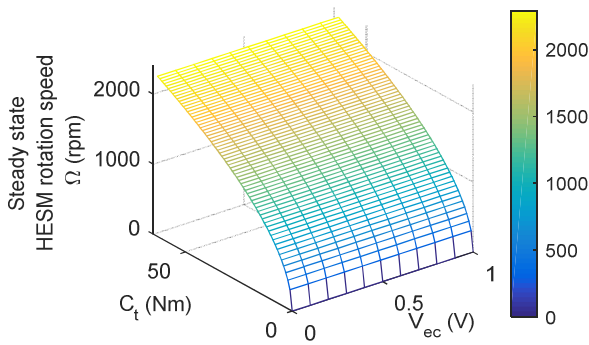


Fig 9: The steady state generator speed versus the turbine torque and the control voltage

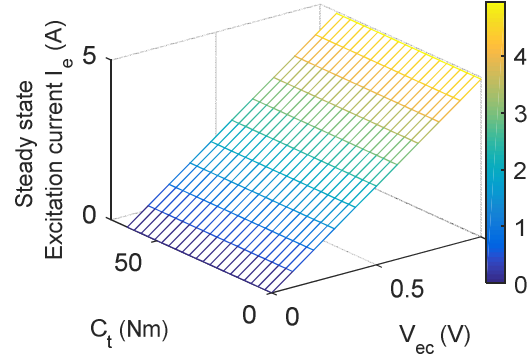


Fig 10: The steady-state excitation current versus the turbine torque and the control voltage

### 3.2. Current loop

The current's loop model was described in [14] and is shown in Fig 11. As one can see, it is a multi-input and nonlinear model. The input  $M\sqrt{3}/L_d \times (v_d - R_s i_d + L_q \omega_i)$  can be considered as a perturbation to design the current's

controller so the current's loop synopsis is as in Fig 12.

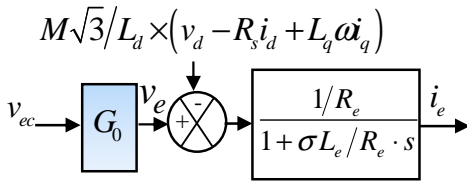


Fig 11: Excitation current model

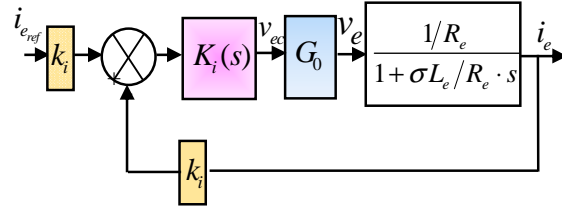


Fig 12: Excitation current loop

Where  $R_s$ ,  $R_e$  are respectively the stator and the excitation resistances,  $\sigma$  is the Blondel coefficient defined by (20).

$$\sigma = 1 - \frac{3M^2}{L_d L_e} \quad (20)$$

$M$  is the mutual inductance and  $L_e$  is the excitation coils inductance.  $G_0$  is a constant gain modeling the DC/DC converter's gain.

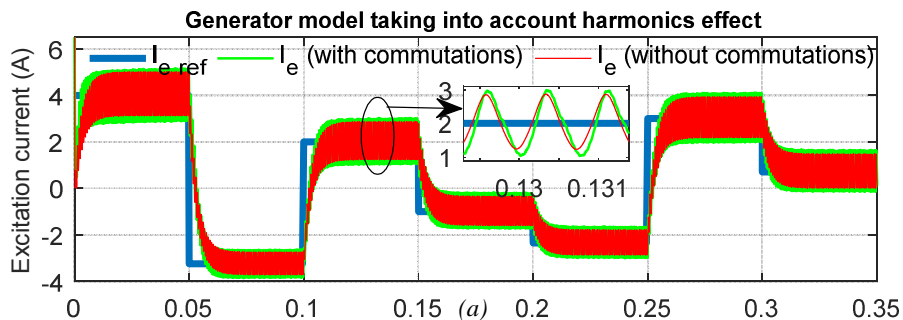
$K_i(s)$  is an integral proportional regulator PI characterized by a time constant  $T_i$  and a gain  $K_i$ . It is designed to satisfy the following specifications:

- A control voltage  $v_{ec}$  less than  $V_{ecm}$  (maximum control voltage);
- A static error trend to zero;
- A closed-loop response time equal to 0.015s which is coherent for a 3kW HESG [29].

A satisfying closed-loop response may be obtained for a damping factor of  $\xi = 0.6$ . Using the relation  $\omega_{0tr} = f(\xi)$ , mixing the damping ratio, the bandwidth and the settling time of a second order system, one can deduce that  $\omega_0$  must be settled around 300rd/s.

$$K_i(s) = K_i \times \left( \frac{1 + T_i s}{T_i s} \right) \quad \text{where} \quad T_i = \frac{\sigma L_e}{R_e} = 0.02s \quad \text{and} \quad K_i = 1.3 \quad (21)$$

The current controller performance is now tested by simulation. As one can see in Fig 12, the commutation effects and the space harmonics are neglected during the controller synthesis procedure: the converter is modeled as a pure gain  $G_0$  and the generator is modeled in the d-q reference frame under an assumption of a first harmonic model. It is then important to test the PI current regulator with an advanced model where these phenomena are taken into account. Simulations show that, for the rated rotation speed of the generator (Fig 8), the harmonics' effects are the more obvious. Indeed, Fig 13 (a) shows that the converters' commutations amplify a bit the rippling of the current's shape but it's not very significant and this phenomenon may be neglected compared to the one caused by the generator's harmonics. Fig 13 (b) proves that the regulator is robust enough to the harmonics' effects. Indeed, the same response is obtained in terms of settling time and overshoot while considering or not the space harmonics effects. Unfortunately, the excitation current's quality is affected, which may badly influence the velocity loop performance since the angular velocity is imposed by the excitation current. For this reason, the consideration of the current's harmonics effect in the design of the velocity controllers is crucial.



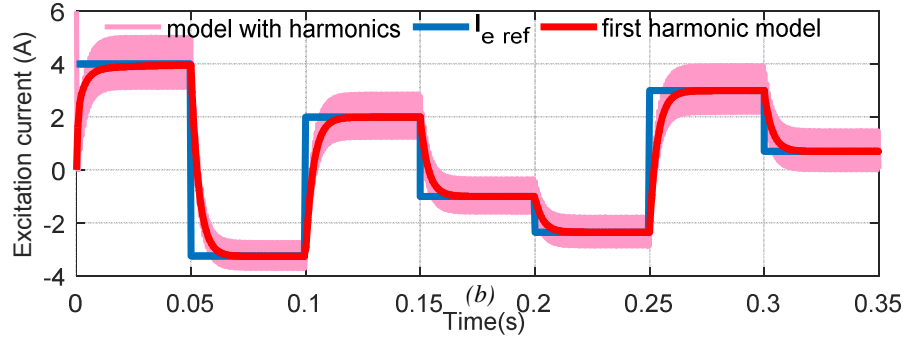


Fig 13: Robustness's analysis of the current controller (simulations)

The test bench of Fig 14 is used for the experimental validation of the current regulator. As the purpose of the present work is to evaluate the contribution of a HESG in wind applications, a WCS emulator with a 3kW HESG generator was constructed. The wind, gearbox, and turbine's rotor are replaced with a 7kW asynchronous motor connected to the HESG through a flywheel Fig 14 (b). This latter was added to the structure in order to increase the emulator total inertia thus emulating faithfully a WCS's dynamic. For the control and measurements, a Humusoft real-time interface and Matlab-Simulink real-time control software are used. The hybrid generator is connected to a resistive load through a full bridge rectifier and a full bridge DC/DC converter controls its excitation coils (Fig 14 (a)).

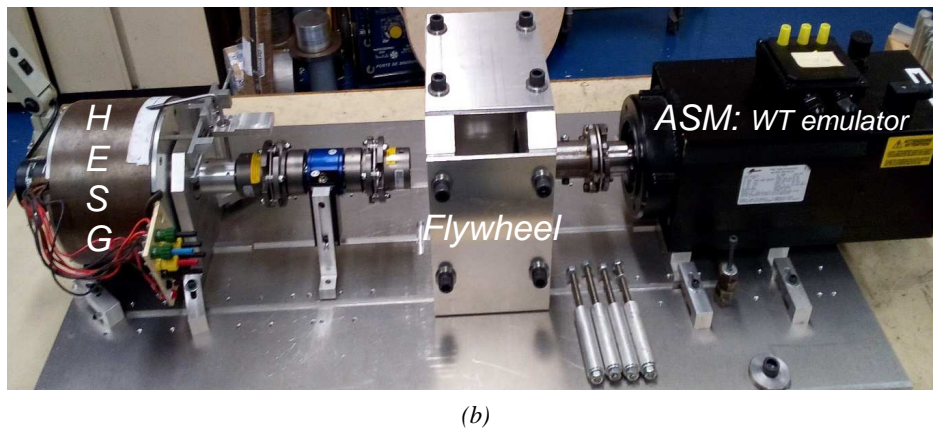
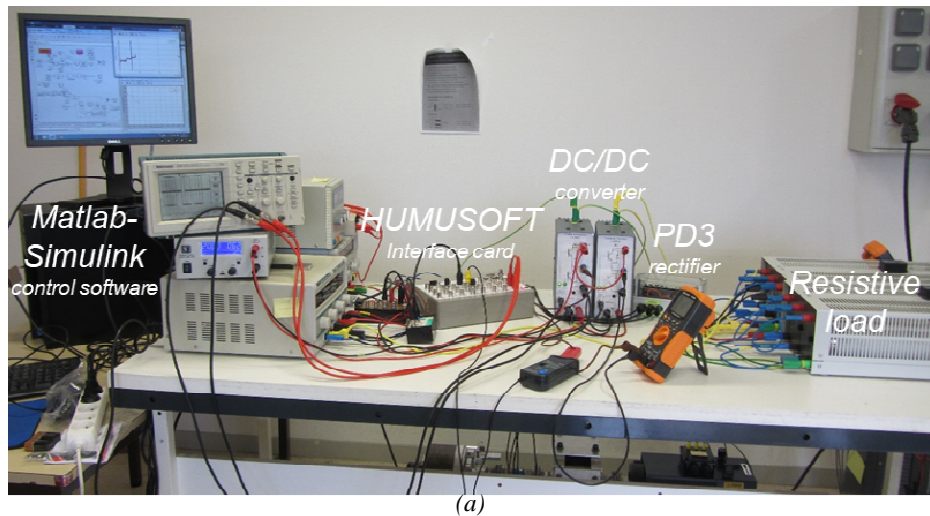


Fig 14: Wind turbine emulator

Very satisfying results, illustrated in Fig 15 and Fig 16, were obtained. The desired closed-loop time response was 0.015s. In practice, the settling time does not surpass 0.011s in the worst, case demonstrating the quality of the current controller. The overshoot is almost null in all cases.

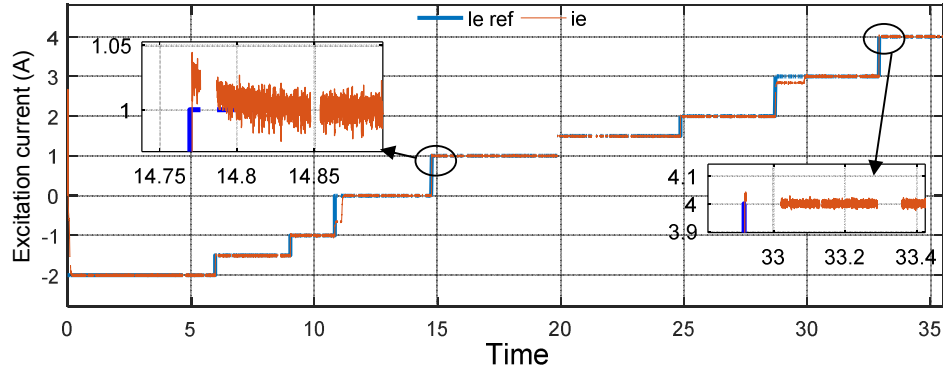


Fig 15: Experimental validation of the current controller (stepped reference)

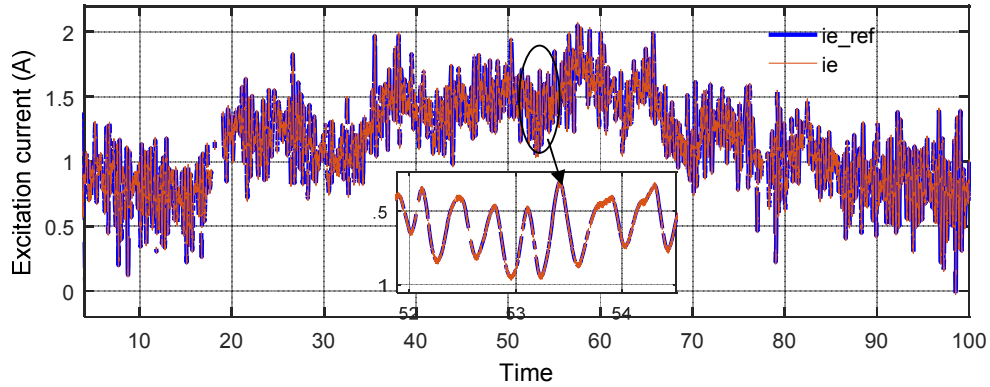


Fig 16: Experimental validation of the current controller (stochastic reference)

### 3.3. WCS linearization

The angular velocity model is given in Fig 17. It is a multi-input and strongly nonlinear model. For the synthesis of both the CRONE and the  $H_\infty$  velocity controllers, a linear model is required. Thereby, the nonlinear model described in Fig 3 and Fig 17 must be linearized. The WCS linearization is performed in zone 2 (Fig 1). In this area, the blades pitch angle  $\beta$  is constant and equal to  $0^\circ$ . The performance coefficient  $C_p$  is also constant and is set to its optimal value [21].

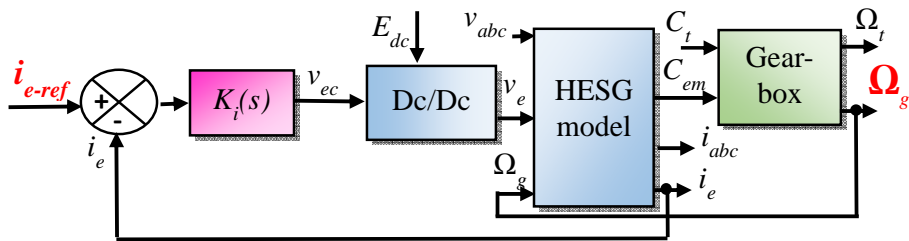


Fig 17: Angular velocity model

An identification process is conducted for four operating points in zone 2 (Fig 18). For a given input signal  $i_{e-ref}$ , corresponding to an operating point, the output  $\Omega_g$  (see Fig 17) is analyzed in terms of overshoot and settling time in order to derive an equivalent linear model.

Fig 1 shows that zone 2 encompasses a wind speed between 3m/s and 11.5m/s and Fig 7 shows that in this zone the optimal turbine rotation speed (respectively the generator rotation speed) is a linear function. Therefore, four operating points well distributed in zone 2 are chosen: the wind speed is set to 4, 6.5, 8.5 and 11 m/s respectively. A set of transfer functions from the input  $i_{e-ref}$  to the output  $\Omega_g$  is then obtained and an average model is selected.

As shown in Fig 18 (c), the consideration of a two masses mechanical model allows a faithful illustration of the flexible coupling between the slow and the fast shaft. For instance, considering a constant wind speed of 8.5m/s, one can notice some vibrations in the angular velocity response. This vibration may decrease the WCS lifetime and even break the shaft. For this reason, the designed controllers have to guarantee a mechanical damping of the WCS.

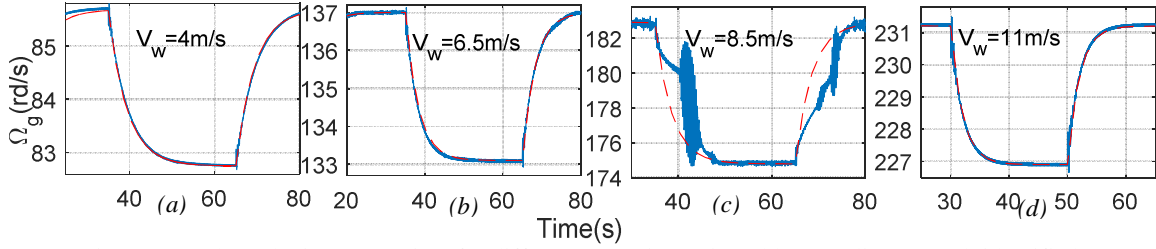


Fig 18: Angular velocity versus time for different operating points (blue: nonlinear – red: identified)

Only three operating points are considered in the identification process because of the uncertainty of the equivalent model computed in Fig 18 (c). Fig 19 shows the Bode diagrams of the local transfer functions  $\Omega_g(s)/i_{eref}(s)$  obtained from the identification process.

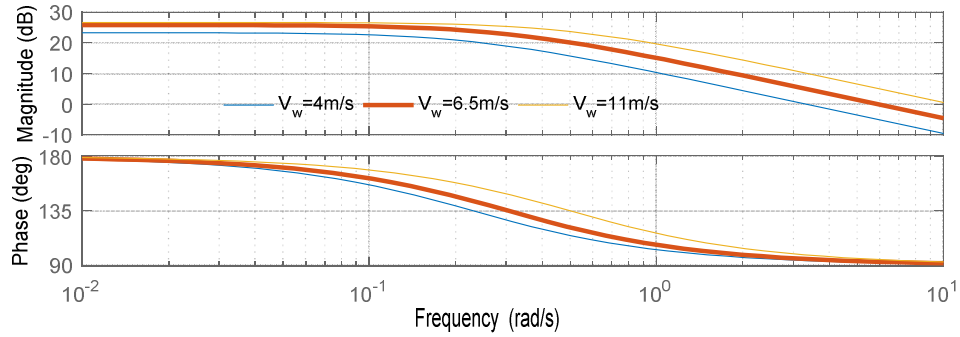


Fig 19: Identified Bode diagrams of  $\Omega_g(s)/i_{eref}(s)$  for different operating points

An average model is selected for 6.5 m/s (Fig 19). It's transfer function is given by (22).

$$H(s) = \frac{\Omega_g(s)}{i_{eref}(s)} = \frac{G_n}{T_n s + 1} = \frac{-19.5}{3.28s + 1} \quad (22)$$

The closed-loop is illustrated by Fig 20 where  $K_{\Omega}(s)$  is the velocity controller to synthesize.

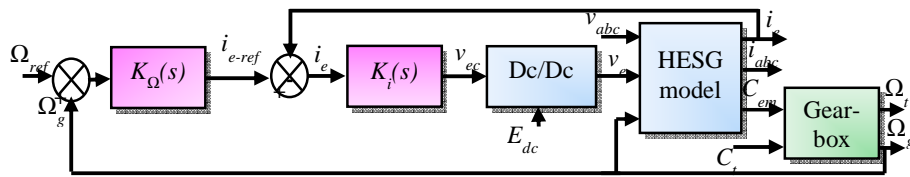


Fig 20: Angular velocity closed-loop

In the present work, the settling time of the angular velocity's closed-loop is set to 6s which is mechanically coherent for a WCS [26]. The inner current loop needs to be at least 10 times faster than the outer velocity loop. This is verified in the present case where the current settling time is about 0.01s. As said previously, the current loop's bandwidth is around 300rd/s. So, a value of 7.7rd/s for the velocity loop's bandwidth is coherent and guarantee a ratio of ten between the two loops.

### 3.4. $H_\infty$ control strategy

The  $H_\infty$  control theory includes two main approaches. The first one is based on closed-loop specifications and it is known as the standard  $H_\infty$  problem. The second one, known as the Normalized Coprime Factors (NCF) robust stabilization problem [35] [36], is based on open-loop specifications and it is considered in the present work.

A synthesis using the NCF method requires that the model to control is described with its prime factors [35]. The normalized left coprime factorization of the nominal model  $\Omega_g(s)/i_{ref}(s)$ , noted  $G(s)$ , is:

$$G(s) = \Omega_g(s)/i_{ref}(s) = M^{-1}(s) \cdot N(s) \quad (23)$$

Where  $N(s)$  and  $M(s)$  are stable transfer functions.

The NCF method gives a controller stabilizing the nominal model  $G(s)$  as well as any model subject to additive uncertainties on  $N(s)$  and  $M(s)$  and belonging to the set of perturbed models written as:

$$\mathbf{G}_\varepsilon = \left\{ \begin{array}{l} G_p = (M + \Delta_M)^{-1}(N + \Delta_N) \\ \|\begin{bmatrix} \Delta_N & \Delta_M \end{bmatrix}\|_\infty \leq \varepsilon \end{array} \right\} \quad (24)$$

Where  $\varepsilon$  denotes the ‘‘size’’ of the uncertainty that the model can handle without being destabilized [36].

The purpose is then to find a single controller  $K(s)$  stabilizing all the plants defined by (24) solving:

$$\inf_{K \text{ stabilising}} \left\| \begin{pmatrix} K \\ I \end{pmatrix} (I + GK)^{-1} M^{-1} \right\|_\infty = \gamma_{\min} = \varepsilon_{\max}^{-1} \quad (25)$$

Where  $\varepsilon_{\max}$  denotes the maximum stability margin.

As the  $H_\infty$  method based on the NCF robust stabilization problem does not address performance directly, pre and post compensators  $W_1(s)$ ,  $W_2(s)$  must be added to the nominal model to give the open-loop the wanted shape. The augmented model is defined by  $G_a(s) = W_2(s)G(s)W_1(s)$ . In the studied case, the model to control is a single input single output (SISO) one, so only a pre-compensator  $W_1(s)$  is necessary. The latter has to ensure that the open-loop has a high gain in low frequencies and a low gain in high frequencies to secure a good reference tracking and a good disturbance rejection. To do so, a proportional integral PI compensator  $W_{PI}(s)$  is selected (26). Indeed, the Bode diagram of Fig 19 shows that in order to ensure a high gain in the low frequencies, the pre-compensator must introduce an integral action. The integral action of  $W_{PI}(s)$  stops around the cut-off frequency of (22) so  $T_1 = T_n$ .

$$W_{PI}(s) = K_1 \cdot \frac{1 + T_1 s}{T_1 s} \quad (26)$$

As one can see in (Fig 19), the natural slope of (22) is -20dB/decade: this is not enough to have a satisfying roll-off. Thus, a low-pass filter is added to the PI in the pre-compensator  $W_1(s)$ . The time constant of the filter must be much smaller than  $T_n$  (a ratio of 10 is usual) to not modify the natural phase margin of (22) around  $w_0$ , so,  $T_f = 0.025T_n$ . Finally,  $W_1(s)$  is given by:

$$W_1(s) = K_1 \cdot \frac{1 + T_1 s}{T_1 s} \cdot \frac{1}{1 + T_f s} \quad (27)$$

The  $H_\infty$  controller is computed for  $G_a(s) = G(s)W_1(s)$  with the Matlab *ncfsyn* function. It is given by (28). As one can see on the Bode plot of the controlled open-loop (Fig 21), a good phase margin of 72.1° is achieved and the crossover frequency is correct. A good maximum stability margin of 0.57 is achieved.

$$K_\infty(s) = \frac{-6.s^3 - 251s^2 - 74.14s - 5.5}{s^4 + 81.7s^3 + 1672s^2 + 246s} \quad (28)$$

### 3.5. CRONE control strategy

CRONE control (French abbreviation of non-integer order robust control) is a frequency approach for a robust control

methodology. In such an approach, the corrected open-loop transfer function has a non-integer (fractional) order, real or complex, that allows defining the optimal open-loop transfer function in terms of overshoot, rapidity and precision with few high-level parameters [37]. The CRONE control includes three generations [37]. The first generation is based on a constant phase of the controller around the desired open-loop cross-over frequency  $w_0$ . The second one is used when there are variations of the gain of the nominal model to control as well as transitional frequencies variations. The third generation should be used when the frequency response of the model to control has uncertainties of various kinds (other than gain and phase types) [37]. Considering the Bode shapes of Fig 19, the second generation seems to be a good choice. It consists in determining, for the nominal state of the plant, the open-loop's transfer function  $\beta(s)$ , defined by (29), which ensures the required specifications [12]:

$$\beta(s) = K_{CRONE}(s) \cdot G(s) = K_u \left( \left(1 + \frac{s}{w_l}\right) / \left(\frac{s}{w_l}\right) \right)^{n_l} \cdot \left( \left(1 + \frac{s}{w_h}\right) / \left(\frac{s}{w_l}\right) \right)^n \cdot \left( 1 / \left(1 + \frac{s}{w_h}\right)^{n_h} \right) \quad (29)$$

Where  $G(s)$  is the uncertain plant model (22).  $K_{CRONE}(s)$  is the controller.  $K_u$  is a constant ensuring unity gain at the desired frequency given by (30) [38].  $w_0$ ,  $w_h$  and  $w_l$  are the transitional high and low frequencies.  $w_l$  and  $w_h$  are geometrically distributed around  $w_0$  and they are calculated as in (31) and (32).  $n_h$ ,  $n_l$  and  $n$  are respectively the order at high frequencies, low frequencies and the order around the crossover frequency (33).

$$K_u = \left(\frac{w_0}{w_l}\right)^{n_l} \cdot \left(1 + \left(\frac{w_0}{w_l}\right)^2\right)^{(n-n_l)/2} \cdot \left(1 + \left(\frac{w_0}{w_h}\right)^2\right)^{(n_h-n_l)/2} \quad (30)$$

$$w_l = w_0 / 10\sqrt{a} \quad \text{and} \quad w_h = w_0 \cdot 10\sqrt{a} \quad (31)$$

$$a = \Delta\beta^{\frac{1}{n}} \quad (32)$$

$$n = (180 - M\phi) / 90 \quad (33)$$

$\Delta\beta$  is the gain variation in the open-loop due to parametric uncertainties and  $M\phi$  is the desired phase margin. It is set to  $85^\circ$  in this case.  $n_h$  is set to 2 to limit the input sensitivity and  $n_l$  is set to 2 ensure zero steady-state error [38] [39].

The constraints defined in the 3.3 section are used in the CRONE toolbox [40] to synthesize the desired controller given by (34). A good phase margin of  $86.4^\circ$  (Fig 21) is achieved around the crossover frequency.

$$K_{CRONE}(s) = \frac{-3.58s^2 - 0.618s - 0.013}{s^3 + 23.9s^2} \quad (34)$$

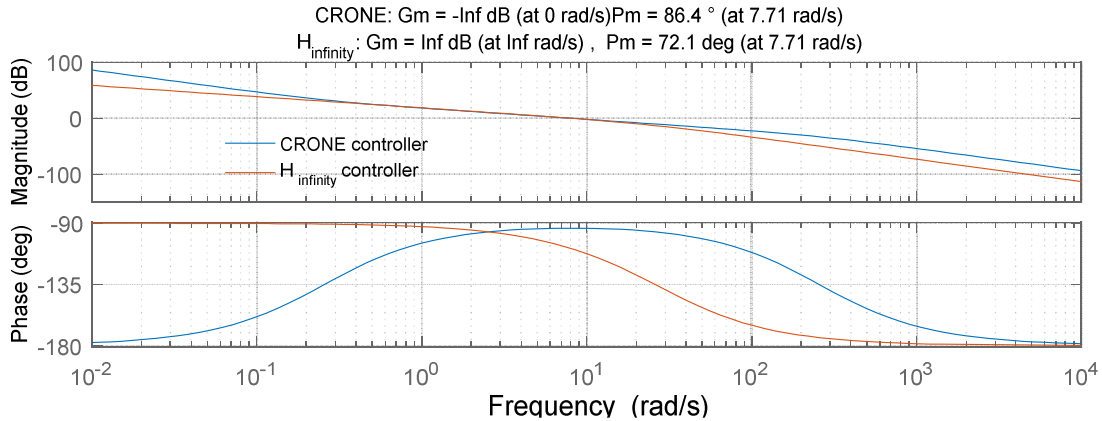


Fig 21: Bode plots of the controlled open-loops

#### 4. Comparison of the two controllers

The performance and robustness of the two regulators are now compared, based on simulations conducted using the WCS model of Fig 3.

#### 4.1. Simulation results

In the present paragraph, the performance of the two controllers is compared in zone 2 and 3 based on simulations conducted on the advanced model of Fig 3 and taking into account the space harmonics and the commutations' effects. In a first test, an artificial wind made of five levels (Fig 22), varying in zone 2, is injected into the nonlinear model of Fig 3 in order to compare the performance of the two controllers to brutal variations of the wind. The results are analyzed regarding the settling time and the overshoot. The same test is done in zone 3 (Fig 25) in order to judge the transient stability of the drive train dynamic.

Fig 23 shows the generator's rotation speeds obtained under a stepped wind profile. It turns out that, with the  $H_\infty$  controller, the static error tends to zero and the oscillations during the transient state are well damped for all the tested operating points with a maximum overshoot of 20%. The CRONE controller causes more overshoot, which can reach 27% in the worst case, showing lesser stability than the  $H_\infty$  controller does. Regarding the settling time, the same performance is registered for the considered speed levels. In the worst-case, it is 6.5s for the two controllers. While a bit higher than expected (6s), this value is quite satisfying. In steady state, the CRONE controller is a bit more precise which justify the small difference in the wind extracted power (Fig 24).

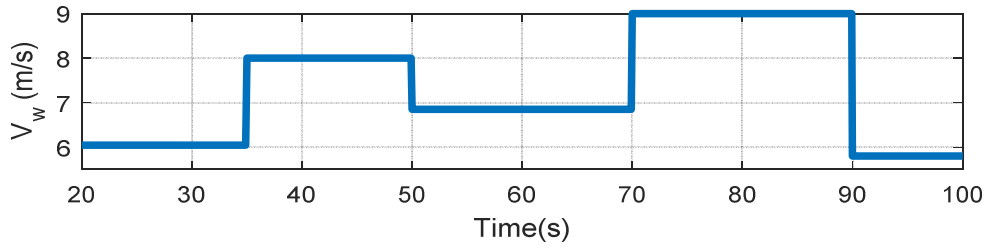


Fig 22: Wind profile

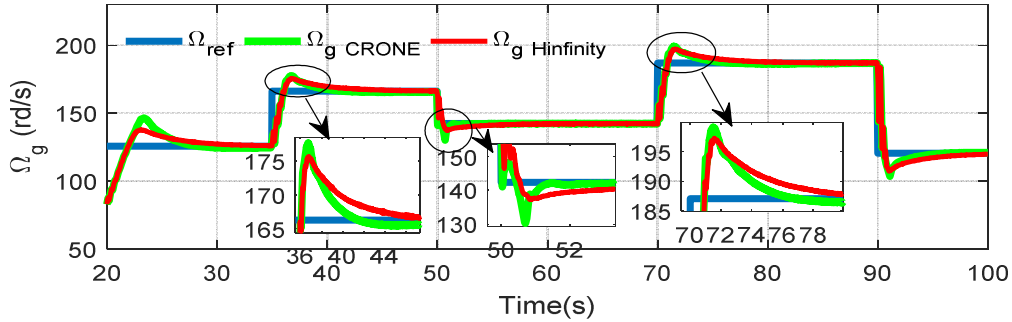


Fig 23: Rotation speed versus time

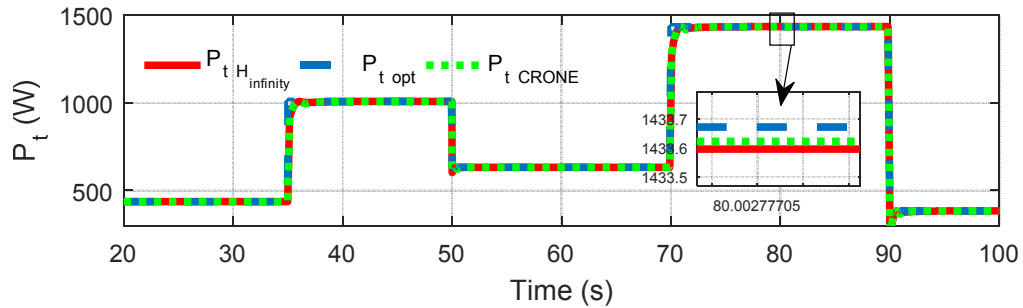


Fig 24: Turbine power versus time

The same test is done in the third zone. The mechanical stress is much greater here. So, it's very important to maintain a constant rotation speed with no rippling. Fig 25 shows the wind profile and Fig 26 shows the velocity response. The slow shaft torque ( $C_b$ ) response as well as the turbine's speed shape, reflect the shaft's twist angle. Thereby they're good indicators of the structural mechanical behavior. It turns out that the CRONE controller provides a better closed-loop

response. The angular velocity rippling is much smaller while using the CRONE controller. Thus, the fluctuations of the torsional torque are lower (Fig 27). Fig 28 illustrates the turbine power, some peaks are observed while changing the wind velocity. These peaks appear only because the wind profile of Fig 25 is very severe. In reality, turbulences can occur but the changes are not quite as tough as the ones imposed by step changes. As one can see in Fig 35, with a stochastic wind profile, the peaks appear no more

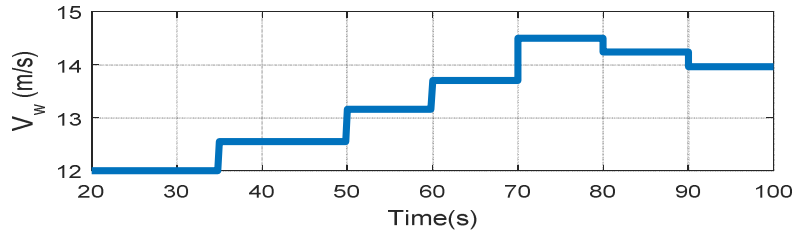


Fig 25: Wind profile

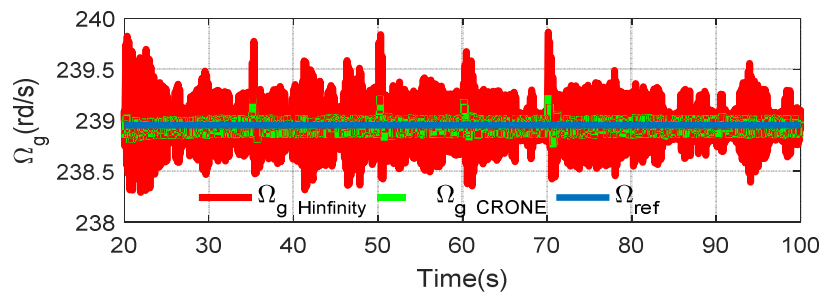


Fig 26: Rotation speed versus time

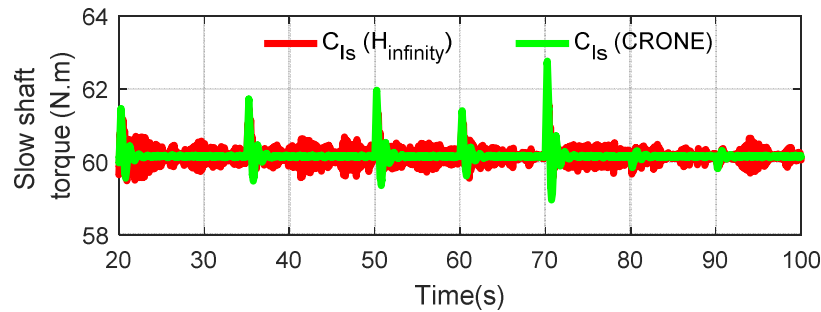


Fig 27: Slow shaft torque versus time

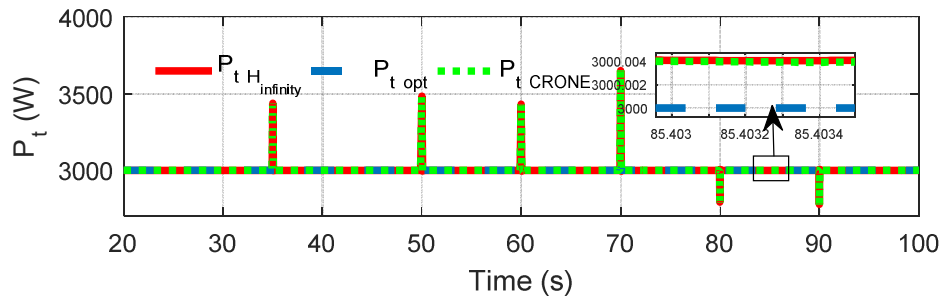


Fig 28: Turbine power versus time

The previous tests are not sufficient to validate the controllers. They do not represent a real wind in a meteorological context. Therefore, the studied architecture is now tested with a stochastic wind profile (Fig 29 and Fig 32). One can

remark that both controllers provide a good reference tracking (Fig 30). In fact, they handle correctly the commutations of the full-bridge rectifier and the DC/DC converter and are robust to the generator's current harmonic perturbations. The CRONE controller is more efficient than the  $H_\infty$  regulator regarding the track of the optimal rotation speed, which justifies the small difference in the turbine-extracted power in Fig 31.

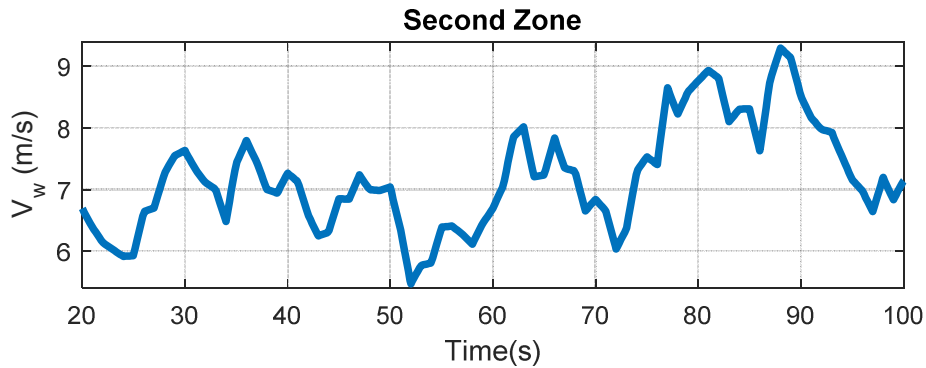


Fig 29: Wind profile

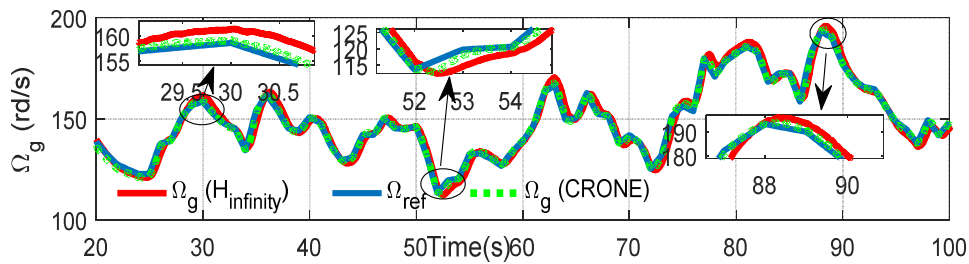


Fig 30: Rotation speed under a realistic wind profile

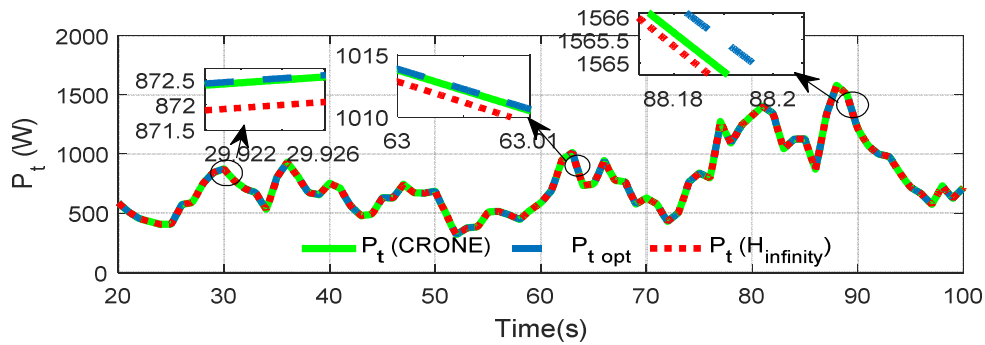


Fig 31: Turbine power versus time

In the third zone, and under a realistic wind profile (Fig 32), the peaks observed in seconds 50 and 70 in Fig 27 do not appear anymore. The CRONE controller is more performant regarding the mechanical vibration and a less oscillatory behavior is observed in Fig 33 and Fig 34: both the slow shaft torque and the rotation speed have better-damped oscillations. Fig 35 presents the turbine power. It can be noticed that the peaks observed in Fig 28 does not appear anymore. The power is limited to 3kW for the whole variation range of the wind speed (from 11.5m/s to 24m/s).

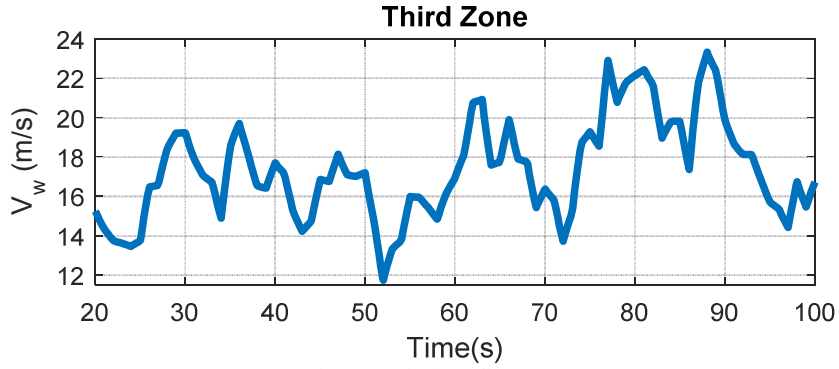


Fig 32: Wind profile

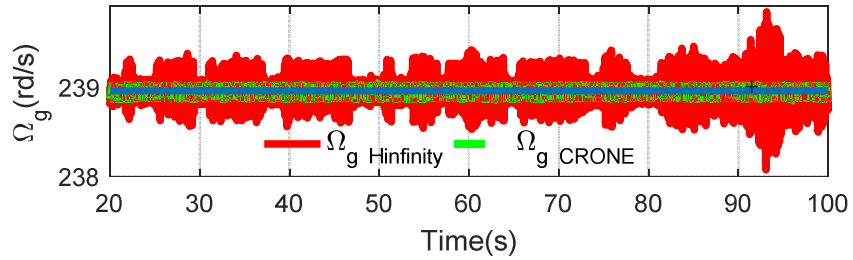


Fig 33: Rotation speed versus time

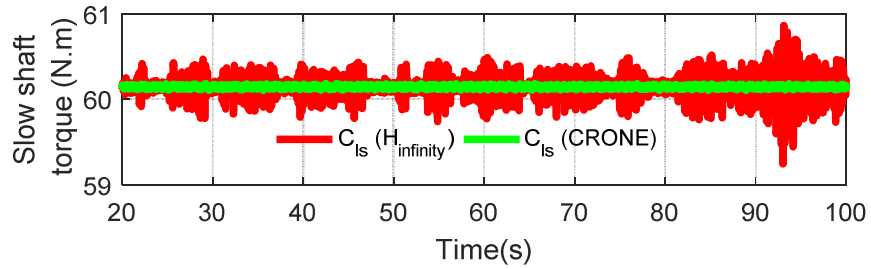


Fig 34: Slow shaft torque versus time

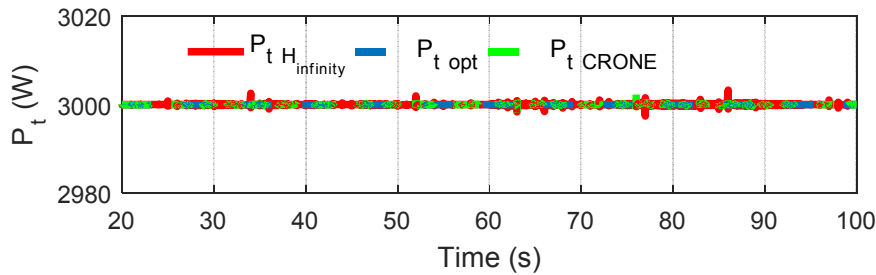


Fig 35: Turbine power versus time

#### 4.2. Robustness analysis

As explained in section 2.1, the mechanical parameters were estimated using the down-scale method and a mean value was calculated. So, they can be considered as quite uncertain. Their uncertainty's range was given in table 1. In the tests thereafter, the robustness of the velocity controllers to these uncertainties is evaluated with simulations conducted on the Simulink model of Fig 3. Here,  $D_{l_{si}}$ ,  $K_{l_{si}}$ ,  $K_{ii}$  and  $J_{ii}$  are the values used in the simulations and  $D_{l_s}$ ,  $K_{l_s}$ ,  $K_t$  and  $J_t$  are the nominal values given in table 1 and used in the linearization process.

Fig 36 proves that the viscous friction and the damping coefficients have no effect on the angular velocity performance even if they are at their maximum uncertainty range. Moreover, the CRONE controller is more performant than the  $H_\infty$

controller regarding the obtained settling time. In this test, the wind velocity is changed from 6.5m/s to 7.5m/s, the  $H_\infty$  controller settling time is around 6s versus 4s for the CRONE controller.

Practically, the same overshoot is obtained with the two controllers: 20% for the CRONE regulator versus 21% for the  $H_\infty$  controller.

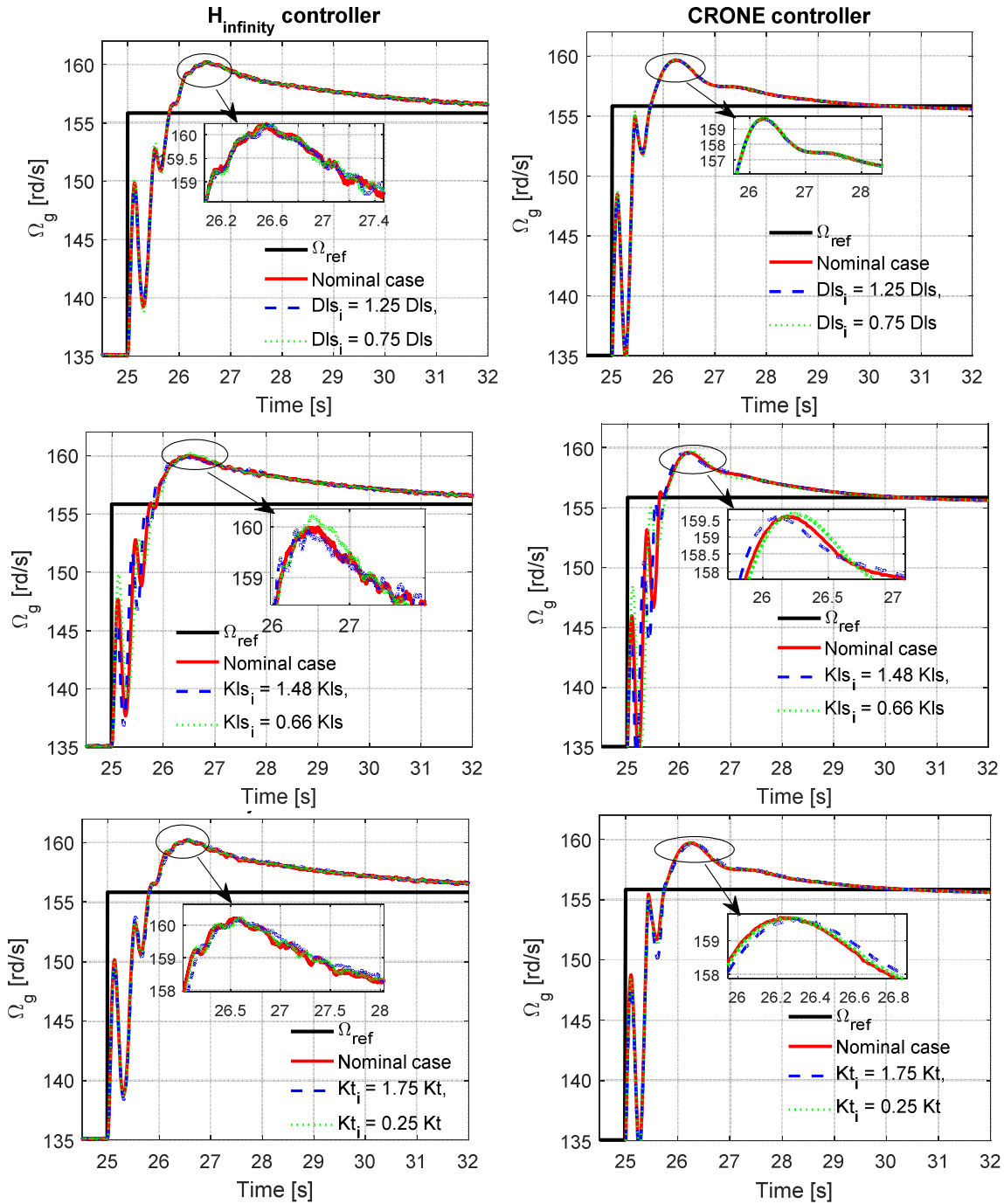


Fig 36: Robustness analysis to mechanical parameters' uncertainty for a wind varying from 6.5m/s to 7.5m/s

The second test focuses on the robustness of the controllers to the electrical parameters' uncertainty. As shown in Table 1, the parameters of the hybrid generator are very uncertain. They may vary with temperature or currents frequencies for instance. Here, the harmonics effects are neglected and the electric parameters vary as follows:

- Case 1: nominal values
- Case 2:  $M=0.8M_e, L_d=0.9L_{dnom}, L_q=0.9L_{qnom}$ .
- Case 3:  $M=0.8M_e, L_d=0.7L_{dnom}, L_q=0.7L_{qnom}, R_s=1.5R_{snom}, R_e=1.5R_{enom}, \phi_a=0.8\phi_{anom}$

In the considered cases,  $M_e, L_{dnom}, L_{qnom}, R_{snom}, R_{enom}$  and  $\phi_{anom}$  are the nominal parameters and  $M, L_d, L_q, R_s, R_e$  and  $\phi_a$  are the ones used for the simulations.

The two controllers are robust to the electrical parameters' variation as shown in Fig 37. The settling time obtained with the CRONE controller (4s) is smaller than the one obtained using the  $H_\infty$  controller (6s) in all cases, but the transitional response of the angular velocity is more violent than the one caused by the  $H_\infty$  controller. However, Fig 30 shows that this vibration does not persist in a realistic wind velocity, so it can be neglected here.

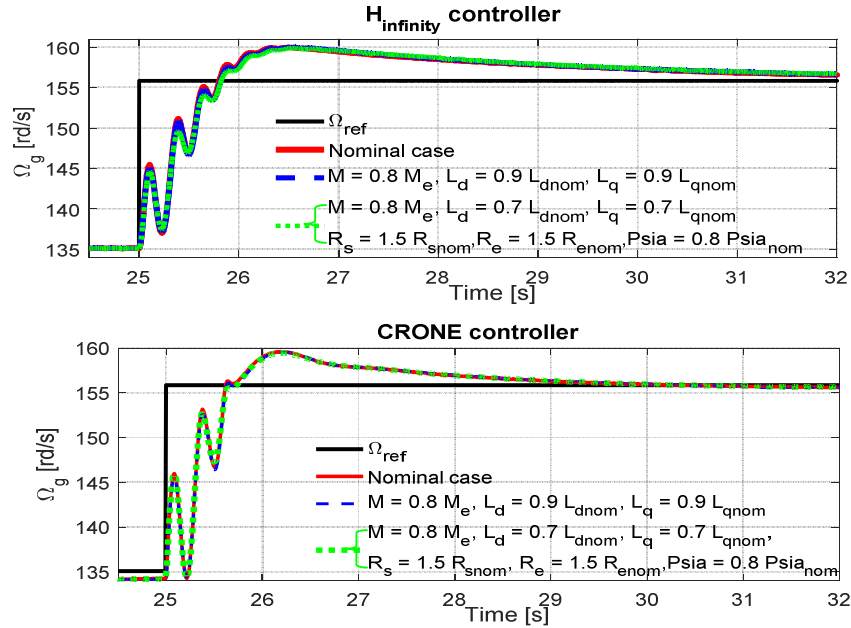


Fig 37: Robustness analysis to electrical parameters' variation for a wind varying from 6.5m/s to 7.5m/s

Fig 38 examines the effects of the space harmonics on the performance of the velocity regulators. The same behavior is observed while considering or not the space harmonics' effects, in terms of overshoot and settling time. Their presence causes a very small rippling of 0.1rd/s on the generator's velocity in steady state. This fluctuation is very small so its impact may be neglected.

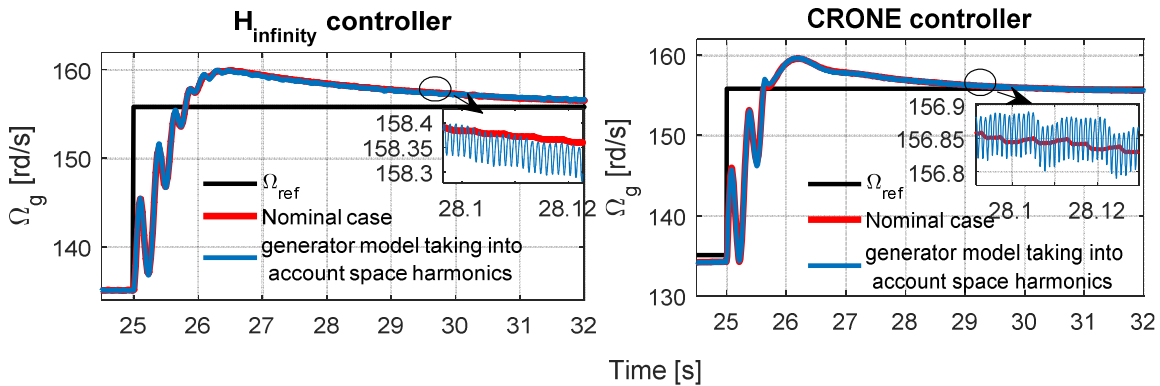


Fig 38: Robustness analysis to space harmonics for a wind varying from 6.5m/s to 7.5m/s

Unlike the test presented in Fig 23, where the wind speed changes brutally, the robustness tests (Fig 36, Fig 37 and Fig 38) are performed around a specific operating point, and in this case, the CRONE controller has a smaller overshoot. In

fact, if the angular velocity's variation  $\Delta\Omega_g$  is small (around a given operation point), the CRONE controller is more robust since its phase margin is greater. However, if the angular velocity's variation is important ( $\Delta\Omega_g \geq 30rd/s$ ), in the case of a gust of wind for example, the  $H_\infty$  controller is more efficient. This is due to the fact that in high frequencies its open-loop gain is smaller (Fig 21) so the  $H_\infty$  controller has a better disturbance rejection.

Finally, the robustness of the two controllers versus the variation of the load is evaluated. Harmonics and switching effects are taken into account. An inductance of 10mH noted  $L_{cnom}$  is connected in series with the resistive load  $R_c$ . Fig 39 shows that the speed regulators handle perfectly the load's variations and the possible induced disturbances are correctly rejected. Such a result could be qualified as very important, since the load evolution mirrors users supply requirements.

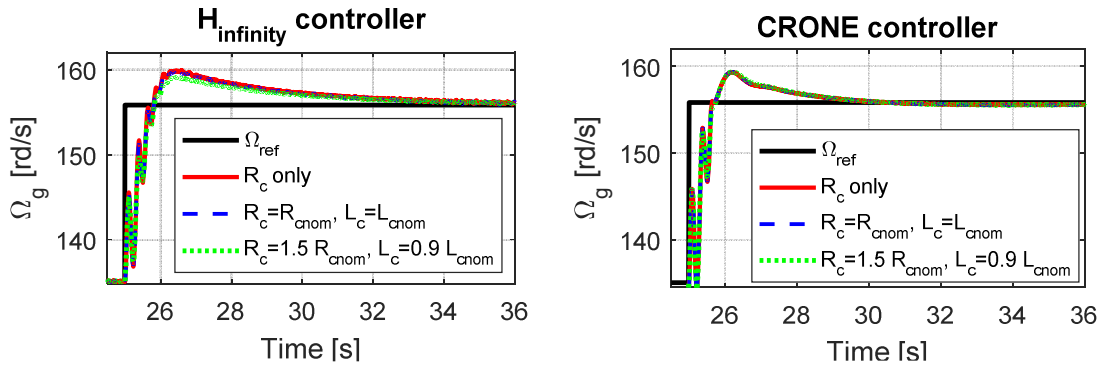


Fig 39: Robustness analysis to the load variation for a wind varying from 6.5m/s to 7.5m/s

The velocity controllers are now evaluated on the test bench of Fig 14. First, a slope-type reference is considered, then, a stochastic one is injected to the emulator. In this case, the average wind velocity's value changes each 20 seconds. It increases from 4m/s to 6.5m/s.

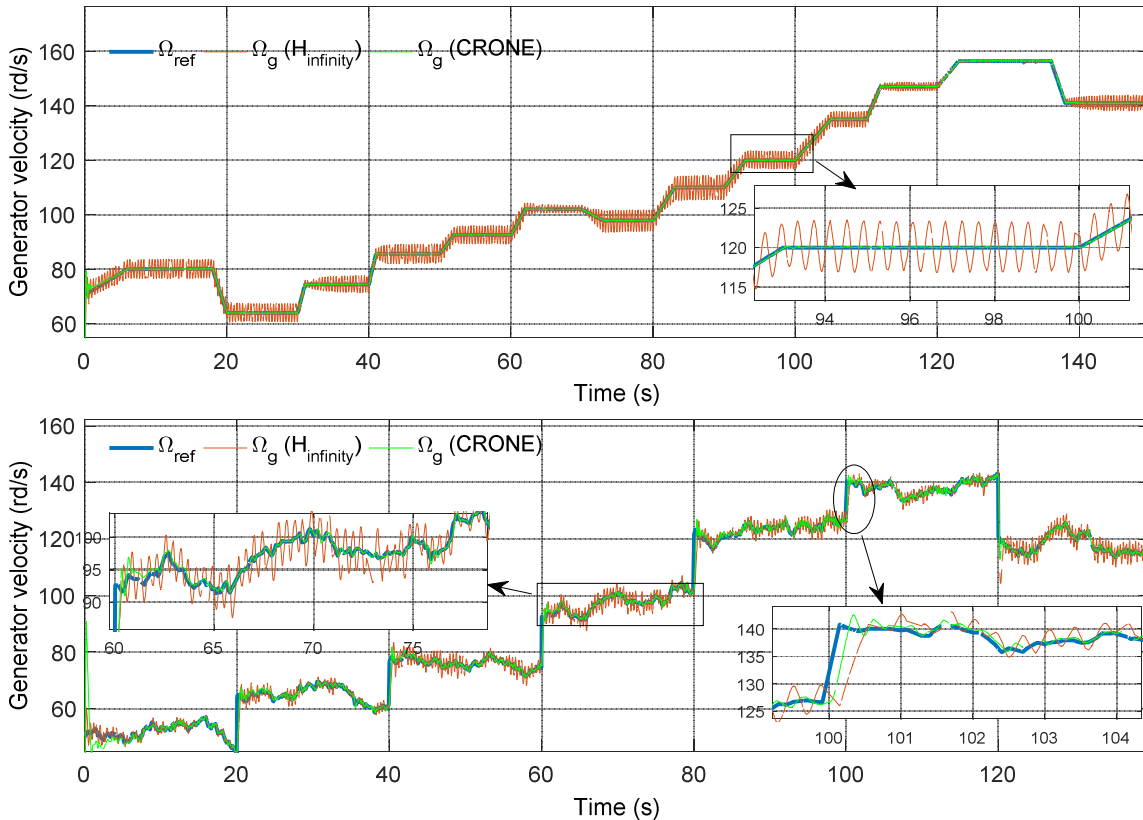


Fig 40: Experimental validation of the velocity regulators

The obtained results prove the efficiency of the CRONE controller. It guarantees a perfect reference tracking (Fig 40). The  $H_\infty$  controller is also validated. However, the angular velocity oscillates around its operation point. These oscillations may reach 8rd/s in the case of a slope-type reference. These experimental tests validate the simulation results and prove that the CRONE controller is mechanically more performant and thereby more adequate for the generator speed's control in a WCS.

## 5. Conclusion and Perspectives

The present paper presents two robust control strategies for a HESG in a wind conversion system connected to an isolated load. The efficiency of the CRONE controller was proved in the small passenger vehicles domain in several works. This motivates the authors to test its performance in the wind energy field. Moreover, the  $H_\infty$  regulator was compared to other robust controllers and its efficiency was proved. Here, the two approaches are introduced and a comparison between a CRONE controller and an  $H_\infty$  controller is presented.

The comparison examines both performance and robustness to the inevitable uncertainties of the parameters of the generator as well as to the space harmonics, the electronic commutations, the wind brutal variations, the mechanical vibrations and the load's variations. The simulation results show that the CRONE regulator has better performance regarding the mechanical parametric uncertainty and the mechanical stress reduction, which testify its robustness. Regarding the optimal rotation speed tracking, similar performances are obtained. However, the  $H_\infty$  controller has a better disturbance rejection. A hybridization of these two control methods may be an attractive solution for an optimal utilization of the WCS. The very good performance of the CRONE controller was also fully validated experimentally under ramped and stochastic references. Future works intend to explore two directions: First, the CRONE controller's robustness to the load variations will be tested by simulations and experimentally. Then, in addition to the advanced electrical model, a complete mechanical model will be implemented using the FAST (Fatigue, Aerodynamic, Structure, and Turbulence) code developed by NREL laboratory [41]. This code models a wind turbine as a combination of rigid and flexible bodies. For now, a 1.5Mw HESG has been dimensioned analytically in order to implement it on this software. Only the current loop of this 1.5Mw machine has been validated.

## Acknowledgment

The authors gratefully acknowledge the contributions of the Foundation Cergy-Pontoise (France) University in the frame of an aid to the development of research projects.

## References

- [1] H. Moradi, G. Vossoughi, Robust control of the variable-speed wind turbines in the presence of uncertainties: A comparison between  $H_\infty$  and PID controllers, *Energy*, vol 90, 2015, pp. 1508-1521.
- [2] A. Sayigh, Renewable energy - the way forward. *Appl Energy*, 1999, pp. 15-30.
- [3] B. Boukhezzar, L. Lupu, H. Siguerdidjane, M. Hand, Multivariable control strategy for variable speed, variable pitch wind turbines, *Renew Energy*. 2007, pp 1273-1287.
- [4] M. Zaibi, G. Champenois, X. Roboam, J. Belhadj, B. Sareni, Smart power management of a hybrid photovoltaic/wind stand-alone system coupling battery storage and hydraulic network, *Math. Comput. Simul.*, 2016.
- [5] M. Hand, Variable-speed wind turbine controller systematic designs methodology: a comparison of nonlinear and linear model-based designs. NREL report. USA, July 1999.
- [6] F.D. Bianchi, R.J. Mantz, C.F. Christiansen, Gain scheduling control of variable-speed wind energy conversion systems using quasi-LPV models, *Control Engineering Practice*, vol 13, 2005, pp. 247-255.
- [7] F.D. Bianchi, H.D. Battista, R.J. Mantz, *Wind turbine control systems: principles modeling and gain scheduling design*. 2nd ed. USA: Springer, 2006.
- [8] K.Z. Ostergaard, Robust, gain-scheduled control of wind turbines, Ph.D. thesis. Denmark: Aalborg University, 2008.
- [9] Z. Wang, Z. Shen, C. Cai, K. Jia, Adaptive control of wind turbine generator system based on RBF-PID neural network, 2014 International Joint Conference on Neural Networks, Beijing, 2014, pp. 538-543.
- [10] M. Soliman, O.P. Malik, D.T. Westwick, Multiple model predictive control for wind turbines with doubly fed induction generators. *IEEE Trans on Sustainable Energy*, vol. 2, July 2011, pp. 215-225.
- [11] A. Dadone, L. Dambrosio, Estimator based adaptive fuzzy logic control technique for a wind turbine-generator system. *Energy Convers Manag*, 2003, pp. 135-53.
- [12] S. Bououden, S. Filali, M. Chadli, Fuzzy predictive control of a variable speed wind turbine, *Energy Procedia*, vol. 42, 2013, pp. 357-366,
- [13] B. Boukhezzar, H. Siguerdidjane, Comparison between linear and nonlinear control strategies for variable speed wind turbines. *Control Eng Pract* 2010, pp. 1357-68.
- [14] K. Berkoune, E. Ben Sedrine, L. Vido, S. Le Ballois, Robust control of hybrid excitation synchronous generator for wind applications, *Math. Comput. Simul.*, Jan 2017, pp 55-75.
- [15] K. Young-Man, Robust data-driven H-infinity control for wind turbine, *Journal of the Franklin Institute*, vol. 353, 2016, pp. 3104-3117.
- [16] A. Benine-Neto, X. Moreau, P. Lanusse, Robust control for an electro-mechanical anti-lock braking system: the CRONE approach, *IFAC-PapersOnLine*, pp. 12575-12581 , 2017.
- [17] J-L. Bouvin, X. Moreau, A. Benine-Neto, A. Oustaloup, P. Serrier, V. Hernette, CRONE control of a pneumatic self-leveling suspension system, *IFAC-PapersOnLine*, pp. 13816-13821, 2017.
- [18] B. Feytout , J. Sabatier, P. Lanusse, M. Lopes, S. Gracia, Maximizing wind turbine production using revisited CRONE control, *European Wind Energy Association Conference (EWEA 2012)*, Apr 2012, Copenhagen, Denmark. pp.1, 2012.
- [19] B.Feytout, P.Lanusse, J.Sabatier, G.Serge, Robust CRONE Design for a variable ratio planetary gearing in a variable speed wind turbine. *Asian Journal of Control*. 2013
- [20] L. Xiping, L. Heyun, Z.Q. Zhu, Y. Chengfeng, F. Shuhua, G.A. Jian, Novel dual-stator hybrid excited synchronous wind generator, *IEEE trans on industry applications*, vol. 45, no. 3, 2009.
- [21] A. Ammar, Modélisation et optimisation d'un générateur synchrone à double excitation de forte puissance. Ph.D. thesis, Ecole centrale de Lille, France, 2013.
- [22] K. Berkoune, E. Ben Sedrine, L. Vido, S. Le Ballois, Control and operating point optimization of hybrid excitation synchronous generator applied for wind application *Electrimacs*, Valence, 2014.
- [23] A. Mseddi, S. Le Ballois, L. Vido, H. Aloui, An integrated Matlab-Simulink platform for a wind energy conversion system based on a hybrid excitation synchronous generator, 11<sup>th</sup> International Conference on Ecological Vehicles and Renewable Energies, Monaco, 2016.
- [24] D. Aguglia, Ph.Viarouge, R. Wamkeue, J. Cros, Determination of fault operation dynamical constraints for the design of wind turbine DFIG drives, *Math. Comput. Simul.*, vol 81, 2010, pp. 252-262.
- [25] M. Rahimi, Drive train dynamics assessment and speed controller design in variable speed wind turbines, *Renewable Energy*, vol. 89, 2016, pp. 716-729.

- [26] H. Li, Z. Chen, Transient stability analysis of wind turbines with induction generators considering blades and shaft flexibility, 33<sup>rd</sup> Annual Conference of the IEEE Industrial Electronics Society, Chongqing, China, 2007, pp. 1604-1609.
- [27] S.M. Muyeen, M.A. Hasan, R. Takahashi, T. Murata, J. Tamura, Y. Tomaki, A. Sakahara, E. Sasano, Comparative study on transient stability analysis of wind turbine generator system using different drive train models, IET Renew.Power Gener, 2007, pp. 131-141.
- [28] N. Srikanth, J.L. Fun, Geometric scaling and long-run reductions in cost: The case of wind turbines. IEEE First International Technology Management Conference, 2011, pp. 691-696.
- [29] P.K. Chaviaropoulos, Similarity rules for W/T up-scaling. CRES, Avr. 2006.
- [30] N. Khezami, Commande multimodèle optimale des éoliennes : application à la participation des éoliennes au réglage de la fréquence. Ph.D Thesis, Lille, France, Tunis, Tunisia, Oct. 2011.
- [31] A. Teninge, Participation aux services système de parcs éoliens mixtes : application en milieu insulaire . Ph.D Thesis, Grenoble, Dec 2009.
- [32] W.E. Leithead, B. Connor, Control of variable speed wind turbines: Dynamic models, International Journal of Control, 2011, pp. 1173-1188.
- [33] R. Abdul Jabbar Khan, M. Akmal, Mathematical modeling of current harmonics caused by personal computers. International Journal of Electrical and Computer Engineering, 2008, pp 3-14.
- [34] L. Leclercq, B. Robyns, J.M. Grave, Control based on fuzzy logic of a flywheel energy storage system associated with wind and diesel generators, Math. Comput. Simul, vol 63, 2003, pp. 271-280.
- [35] R. Mbayed, G. Salloum, L. Vido, E. Monmasson, M. Gabsi, Hybrid excitation synchronous generator in embedded applications: modeling and control, Math. Comput. Simul, 2012.
- [36] L. Vido, Etude d'actionneurs électriques à double excitation destinés au transport : dimensionnement de structures synchrones. Ph.D Thesis, ENS Cachan, France, 2004.
- [37] A. Mseddi, S. Le Ballois, H. Aloui, L. Vido, Comparative study of two robust control strategies for a wind conversion system based on a hybrid excitation synchronous generator, Electrimacs, Toulouse, 2017.
- [38] S. Ganjefar, A. A. Ghassemi, M. M. Ahmadi, Improving efficiency of two-type maximum power point tracking methods of tip-speed ratio and optimum torque in wind turbine system using a quantum neural network, Energy, vol 67, pp. 444-453, 2014.
- [39] D. McFarlane, K. Glover, Robust controller design using normalized coprime factor plant descriptions, lecture notes in control and information sciences, springer Verlag, 1990.
- [40] N. Ouddah, M. Boukhifir, A. Chaibet, E. Monmasson, Fixed structure  $H_\infty$  loop shaping control of switched reluctance motor for electrical vehicle, Math. Comput. Simul, 2015.
- [41] J. Sabatier, P. Lanusse, B. Feytout, S. Gracia, CRONE control based anti-icing/deicing system for wind turbine blades. Control Engineering Practice, 2016, pp. 200-209.
- [42] F. Christophy, X. Moreau, R.A.Z. Daou, Temperature control of a diffusive medium using the second generation CRONE control. Technological Advances in Electrical, Electronics and Computer Engineering, 3<sup>rd</sup> International Conference, Beirut, 2015, pp. 195-200.
- [43] A. Morand, X. Moreau, P. Melchior, M. Moze, Robust cruise control using CRONE approach. 6<sup>th</sup> Workshop on Fractional differentiation and its applications part of 2013, IFAC Joint Conference SSSC, FDA, TDS, Grenoble, France, 2013.
- [44] Web-site: <http://cronetoolbox.ims-bordeaux.fr>, Dec 2016.
- [45] D.J. Malcolm, A.C. Hansen, WindPACT Turbine rotor design study, June 2000 - June 2002.